Chemical Physics Letters 683 (2017) 240–246

Contents lists available at ScienceDirect

Chemical Physics Letters

journal homepage: www.elsevier.com/locate/cplett

Research paper

Pursuit of the Kramers-Henneberger atom

Qi Wei [a], Pingxiao Wang [b], Sabre Kais [c,d], Dudley Herschbach [e,f,*]

[a] State Key Laboratory of Precision Spectroscopy, East China Normal University, Shanghai 200062, China
[b] Institute of Modern Physics, Department of Nuclear Science and Technology, Fudan University, Shanghai 200433, China
[c] Department of Chemistry and Physics, Purdue University, West Lafayette, IN 47907, USA
[d] Qatar Environment and Energy Research Institute, HBKU, Qatar Foundation, Doha, Qatar
[e] Department of Chemistry and Chemical Biology, Harvard University, Cambridge, MA 02138, USA
[f] Institute for Quantum Science and Engineering, Texas A&M University, College Station, TX 77843, USA

ARTICLE INFO

Article history:
Received 29 December 2016
In final form 7 February 2017
Available online 12 February 2017

Keywords:
Superintense laser
Quiver motion
Neutral atom acceleration
Ponderomotive force
Kramers-Henneberger atom

ABSTRACT

Superstrong femtosecond pulsed lasers can profoundly alter electronic structure of atoms and molecules. The oscillating laser field drives one or more electrons almost free. When averaged over, the rapid oscillations combine with the static Coulomb potential to create an effective binding potential. The consequent array of bound states comprises the "Kramers-Henneberger Atom". Theorists have brought forth many properties of KH atoms, yet convincing experimental evidence is meager. We examine a remarkable experiment accelerating atoms (Eichmann et al., 2009). It offers tantalizing evidence for the KH atom, with prospects for firm confirmation by adjustment of laser parameters.

1. Introduction

An intriguing prediction of theory treating electronic properties of atoms subjected to superintense, high-frequency laser fields is that the ionization probability decreases as the laser intensity increases [1–3]. This seeming paradox occurs because the "laser-dressed" atom acquires an effective binding potential formed by interaction of the rapidly oscillating laser field with the static Coulomb potential. The stabilization against ionization even extends to multiply charged anions of hydrogen [4], and anions of other atoms [5–7] as well as positronium [8] and some simple diatomic molecules [9,10], including H_2^+, H_2, and He_2. Even more striking is a theoretical demonstration, using a carefully devised laser dressing that counteracts Coulombic repulsion, to form a metastable HD^{2+} molecule [11]. That emulates a juggler, balancing a stick on the tip of a finger. Kindred physics producing long-lifetime stable motions by combining rapidly oscillating and static potentials appears in the inverse pendulum of Kapitza [12], in the Paul mass filter [13], and in Hau guided matter waves [14].

In strong field laser dressing of a neutral atom, one or more electrons undergo quiver motion that follows the laser oscillations, becoming almost free but still weakly bound to the parent ionic core. A procedure termed high frequency Floquet theory (HFFT) adopts the reference frame of the oscillating electron, in which the electron is at rest, and then averages the interaction with the core over a laser oscillation cycle [1]. The net effective binding potential, viewed from the electron rest frame, defines the "Kramers-Henneberger Atom" [15,16]. An excellent overview of the KH atom and its evolution is given in a recent thesis by Maria Richter [17]. The KH atom provides realistic bound states and electron distributions only if the harmonics of the oscillating interactions (which average to zero) can be neglected. That holds for high frequencies, particularly in the ultraviolet range [18]. Yet the KH atom is now considered a suitable approximation even for relatively low frequencies in the infrared range, especially for very strong laser fields, as HFFT analysis [19] has been confirmed by *ab initio* results [20,21].

Abundant theory employing HFFT and KH methods reaches back three decades [1–3,17], but experimental confirmation of adiabatic stabilization against photoionization proved elusive. In order to attain the requisite intensity, a pulsed laser had to be used. During the rising edge of the pulse, most target atoms were ionized, so few if any survived intact when the pulse intensity had climbed to the stabilization regime. This was termed the "death valley" problem. The first definitive experimental evidence for stabilization was obtained two decades ago, using a circular Rydberg 5g state of Neon [22]. A large fraction survived traversing death

* Corresponding author at: Department of Chemistry and Chemical Biology, Harvard University, 12 Oxford St., Cambridge, MA 02138, USA.
E-mail addresses: qwei@admin.ecnu.edu.cn (Q. Wei), wpx@fudan.edu.cn (P. Wang), kais@purdue.edu (S. Kais), dherschbach@gmail.com (D. Herschbach).

http://dx.doi.org/10.1016/j.cplett.2017.02.017
0009-2614/

valley because the minimum lifetime for ionization exceeded the pulse rise time, and no further ionization occurred when the pulse peak intensity was increased above 60 TW/cm^2. Yet, a decade-long hiatus ensued until more experiments pertaining to inhibition of ionization in strong laser fields emerged [23–28]. Those results stimulated recent theory that focuses on other properties associated with the KH atom. Thereby means have been demonstrated to directly image, by photoelectron spectroscopy, the exotic electronic structure of the KH atom [20]. Also, it has been shown that by suitably shaping the driving laser pulses, signatures of the excited KH states can be revealed in the Kerr effect response [21].

Here we discuss a remarkable experiment, by Eichmann et al. [24], employing intense short-pulse IR laser fields that produced unprecedented acceleration of neutral He and Ne atoms, up to 10^{15} m/s^2. It offers another source of evidence for the KH atom, not previously examined. The major contribution to the acceleration was identified as the ponderomotive (PM) force on excited electrons bound in Rydberg orbits that survive long enough to enable the atoms to reach the detector. However, the observed velocities lie somewhat above the theoretical prediction. We find that in addition to the PM potential there exists a smaller but significant term that comes from the binding energy of the KH atom. Including this KH term brings the calculated maximum velocities to a close match with the experimental results over the full range of laser pulse durations. It appears feasible to increase the laser frequency enough so the KH force becomes much larger than the PM force.

2. The ponderomotive force

Fig. 1 displays essential components of the experiment [24]. During each laser pulse the quivering electron behaves as a quasi-free electron, but after the pulse ends the Coulombic attraction to its parent ion core recaptures the electron into a Rydberg state. However, during the pulse, the quasi-free electron is subject to the ponderomotive force exerted by the intensity gradient in the focused laser beam. The subsequent reattachment of the electron

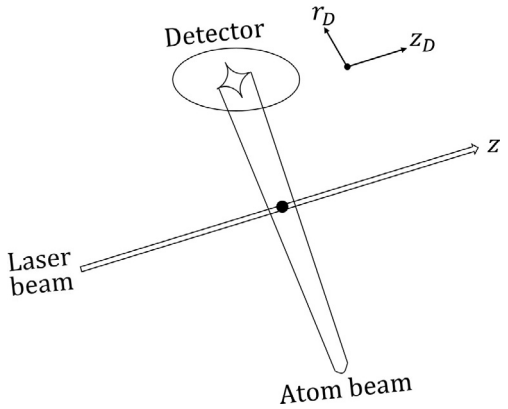

Fig. 1. Schematic sketch of experiment [24]. A linearly polarized Ti:sapphire laser beam with a repletion rate of 500–1000 Hz, a variable pulse width of τ_{FWHM} = 40–120 fs and pulse energies up to 2.5 mJ, and peak intensity up to 6×10^{15} W cm^{-2}, enters a vacuum chamber. There it is focused into a perpendicularly crossed atomic beam (~6 mm wide, traversing the focal plane at z = 0, marked by a dot). Atoms that are excited (but not ionized), during the laser pulse duration, travel on to a multichannel position detector (3.8 cm downstream) that responds only to atoms with excitation energies of more than ~5 eV. For He and other rare gas atoms the laser excitation produces mainly Rydberg states [23], which partially decay to metastable states that live long enough to reach the detector. The distribution of excited atoms on the detector and time-of-flight data reveal the laser induced forces. *Atomic units:* 1 au for distance is a bohr unit (0.0529 nm); for energy a hartree unit (27.2 eV); for laser intensity 3.51×10^{16} W cm^2; and for frequency 6.58×10^{15} Hz, corresponding to wavelength of 45.5 nm.

to the ion core thus produces acceleration of the neutral atom, albeit less strong in the ratio of the atom mass to the electron mass. Thereby a substantial momentum transfer to the atom occurs despite the short interaction time in the laser pulse, in the femtosecond range. That momentum transfer shows up in the distribution of excited atoms that arrive at the detector. If no momentum had been transferred (laser off), the image of the distribution on the detector would extend (along the z_D-axis) parallel to the laser beam direction (z-axis) due to the atom beam width, but with a very narrow radial spread (r_D-axis) comparable to the laser beam waist. The actual observed image [24] exhibits a strikingly large radial distribution of excited atoms with a strong maximum in the laser focal plane (z = 0).

We now outline the pertinent theory. Starting from the time-dependent Schrödinger equation for a one-electron atom in the velocity gauge and laboratory frame:

$$\left[\frac{1}{2}\left(\boldsymbol{p}-\frac{1}{c}\boldsymbol{A}(t)\right)^2+V(r)\right]\Psi = i\frac{\partial\Psi}{\partial t} \tag{1}$$

We use conventional atomic units (au), with Planck's constant, the electron charge and its mass all set to unity ($\hbar$ = e = m_e = 1). Numerical values are in the caption to Fig. 1. By applying the KH transformation in the nonrelativistic regime [16,29], the Hamiltonian can be recast as:

$$\hat{H} = \frac{\boldsymbol{p}^2}{2} + V(\boldsymbol{r}+\boldsymbol{\alpha}) + \frac{\boldsymbol{A}^2}{2}, \tag{2}$$

with $\boldsymbol{p}$ the momentum, $\boldsymbol{A}(\mathbf{t})$ the vector potential, and $\boldsymbol{\alpha}(\mathbf{t})$ the quiver motion of the electron relative to the laboratory frame of a classical free electron in the laser field. In the KH frame, $V(\boldsymbol{r}+\boldsymbol{\alpha})$ is the potential due to interaction of the electron with the nucleus or to an atomic core, which corresponds to $V(\boldsymbol{r})$ in the lab frame. Since only one electron is excited, the interaction between the loosely bound electron and the atomic core is modeled by:

$$V(\boldsymbol{r}) = -\frac{1}{r}(1+e^{-\delta_0 r}), \tag{3}$$

$V(\boldsymbol{r})$ is comprised of a long range Coulomb potential and a short range Yukawa type potential. Theparameter $\delta_0 = 2.13$ and 2.32 (atomic units) for He and Ne atoms, respectively [30]. The KH atom is subject to a linearly polarized laser pulse propagating along the z direction and the corresponding vector potential has the form:

$$\boldsymbol{A}(t) = \frac{E_0(\boldsymbol{r},t)}{\omega}\sin[\omega(t-z/c)] \tag{4}$$

where $E_0(\mathbf{r}, t)$ is the slowly varying laser electric field amplitude and ω its frequency. The cycle-averaged vector potential term in the Hamiltonian is the ponderomotive potential: $\hat{H}_{PM} = \langle A^2/2\rangle = |E_0(\boldsymbol{r},t)|^2/4\omega^2$, which represents the kinetic energy due to oscillation of the electron in the laser field. The other terms in the Hamiltonian, denoted $\hat{H}_{KH}$, represent the KH atom. Then the force imposed on the atom is:

$$F = -\nabla\langle\hat{H}\rangle = -\nabla\langle\hat{H}_{KH}\rangle - \frac{1}{4\omega^2}\nabla|E_0(\boldsymbol{r},t)|^2 \tag{5}$$

The last term in Eq. (5) is the ponderomotive force,

$$F_{PM} = -\nabla\langle\hat{H}_{PM}\rangle = -\frac{1}{4\omega^2}\nabla|E_0(\boldsymbol{r},t)|^2 \tag{6}$$

governed by the gradient of the spatial intensity distribution and its temporal dependence. For a linearly polarized laser beam with a Gaussian profile; in cylindrical coordinates:

$$I(r,z,t) = |E_0(\boldsymbol{r},\mathrm{t})|^2 = I_0(w_0/r_0)^2\,\exp\left[\frac{-2r^2}{r_0^2}\right]f(t) \tag{7}$$

The laser pulse is so short the atom does not move significantly during the pulse. Hence, the pertinent time dependence is just the pulse envelope, which is taken to be Gaussian: $f(t) = \exp(-t^2/\tau^2)$, with $\tau = \tau_{FWHM}/(2\ln 2)^{1/2}$; the full pulse duration is $\pi^{1/2}\tau$. In the spatial distribution, I_0 represents the magnitude of the field intensity in the center of the laser focus; $r_0 = w_0[1 + (z/z_R)^2]^{1/2}$, with w_0 the beam waist; z_R is the Rayleigh length, the distance along the laser beam direction from the waist (at z = 0 at the focal plane) to where the cross section has doubled. Typically, for lasers, z_R is 100-fold or more larger than w_0. The gradient of I(r, z) and thus the PM force in the beam direction is much smaller than in the radial direction, so can be neglected [24,31]. Thus, the radial PM force exerted on atoms within the laser beam is simply

$$F_{PM} = -\frac{dI}{dr}\cdot\frac{1}{4\omega^2} = \frac{r}{r_0^2}\cdot\frac{1}{\omega^2}\cdot I(r,z,t) \tag{8}$$

It is maximal for atoms located in a small region within the laser beam: on its focal plane, z = 0, and at a "half-beam" radial site, $r = w_0/2$. That maximal location does not change with the laser frequency. As well as dropping off rapidly outside the focal plane, the PM force declines steeply for both $r > w_0$ and $r < w_0/5$, then vanishes at center of the laser beam, r = 0. The PM force is the same in classical and quantum mechanics, whereas the KH term arises from quantum mechanics.

3. The KH force

To assess the contribution from $-\nabla\langle\hat{H}_{KH}\rangle$, we assume that the quantum state of the KH atom evolves adiabatically, which holds when the field amplitude varies slowly during the laser pulse [23]. Then the time-dependent dynamics can be converted into a quasistationary Schrödinger equation [1,3,16]:

$$\left[\frac{\boldsymbol{p}^2}{2} + V_0(\boldsymbol{r},\alpha_0)\right]\Phi_{KH} = \in_n(\alpha_0)\Phi_{KH} \tag{9}$$

Here the interaction potential has been dressed by averaging the electron quiver motion over a laser oscillation cycle:

$$V_0(\boldsymbol{r},\alpha_0) = \frac{1}{2\pi}\int_0^{2\pi} V[\boldsymbol{r} + \boldsymbol{\alpha}(\xi/\omega)]d\xi \tag{10}$$

with $\boldsymbol{\alpha}(t) = \alpha_0\cos(\omega t)x$. The amplitude, $\alpha_0 = \sqrt{I}/\omega^2$ for a linearly polarized laser field, is governed by the laser frequency ω, which is constant, and the intensity $I = |E_0|^2$. The eigenenergies $\in_n$ are functions only of α_0 and the corresponding states are termed KH states.

As noted in the Introduction, Eq. (7), often used in treating high-frequency fields, has recently been deemed a suitable approximation for lower-frequency fields with laser intensities at which the quivering electron becomes nearly free [19–21]. Accordingly, we can approximate $\langle\hat{H}_{KH}\rangle$ by $\in_0(\alpha_0)$. The ground KH state is only weakly bound but much more than higher states. The radial force arising from the KH term is obtained from:

$$F_{KH} = -\nabla\langle\hat{H}_{KH}\rangle = -\frac{\partial\in_0}{\partial\alpha_0}\cdot\frac{\partial\alpha_0}{\partial I}\cdot\frac{\partial I}{\partial r} \tag{11}$$

The two factors, $\partial\alpha_0/\partial I = \alpha_0/2I$ and $\partial I/\partial r = -4(r/r_0^2)I = -4\omega^2 F_{PM}$, are available explicitly, but $d\in_0/d\alpha_0$ requires solving Eq.(9) numerically. Thus, the KH force is given by

$$F_{KH} = -\nabla\langle\hat{H}_{KH}\rangle = \frac{2r}{r_0^2}\cdot\frac{\sqrt{I(r,z,t)}}{\omega^2}\cdot\frac{d\in_0}{d\alpha_0} \tag{12}$$

In an Appendix we provide a formula for $d\in_n/d\alpha_0$ fitted to the numerical results. Fig. 2 compares $\in_0$ and $\partial\in_n/\partial\alpha_0$ for He and Ne atoms with those [1] for the H atom. The three curves nearly overlap for $\alpha_0 > 4a.u.$ and separate from H only for $\alpha_0 < 4a.u.$ As α_0 increases, $\in_0$ decreases monotonically, hence the ground state KH atom is a low-field seeker. The slope $d\in_n/d\alpha_0$ is much larger for the ground state than for the higher states in the range of α_0 that contributes most to F_{KH}, another reason for dealing here just with the ground state.

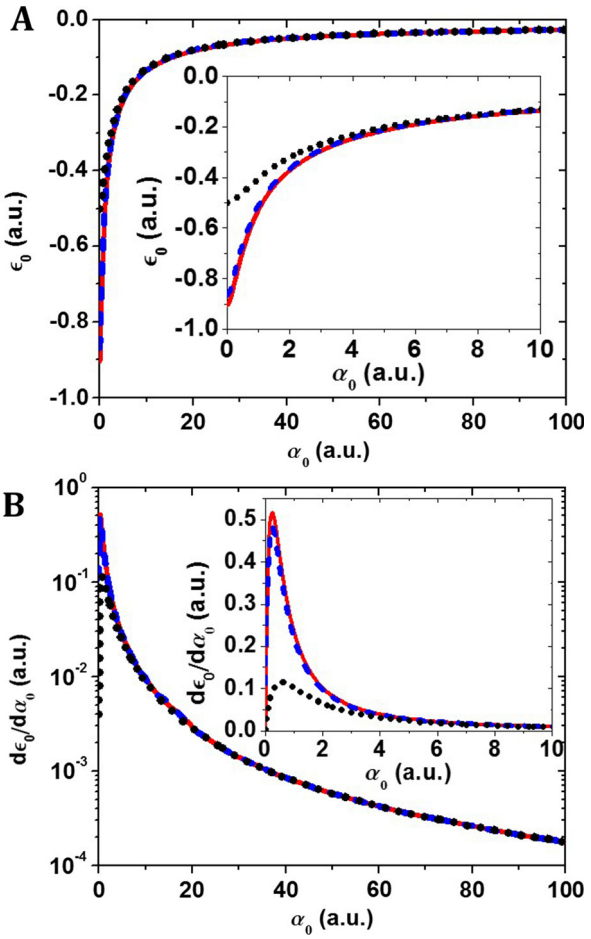

Fig. 2. (A) Ground state energy $\in_0$ and (B) slope $d\in_0/da_0$ as functions of the quiver amplitude α_0 for KH state atoms. Full curves are for He (red); dashed for Ne (blue); dotted for H atom (black). (For interpretation of the references to colour in this figure legend and subsequent others, the reader is referred to the web version of this article.)

In contrast to the PM force, the maximal KH force occurs at z = 0 and near $r = 2w_0$ for $\omega = 0.056$ a.u. ($\lambda = 814$ nm) and shifts downwards below $r = 1.5w_0$ as the frequency increases toward 0.224 a.u. ($\lambda = 203$ nm).

Fig. 3 displays, in panel (A) the temporal variation of the quiver amplitude during the laser pulse intensity envelope, $f(t) = \exp(-t^2/\tau^2)$, with constant pulse length, $\tau_{FWHM} = 100$ fs, and constant peak intensity, $I_0 = 0.080$ a.u. for three frequencies. The corresponding PM and KH forces are shown in panel (B) that would be exerted on atoms during the laser pulse. These were derived from Eqs. (8) and (12) along with f(t), for atoms located at maximal force positions of (r, z) distributions within the laser beam (*cf.* Figs. 4 and 5). At frequency #1 ($\omega = 0.056$ a.u.; $\lambda = 814$nm), the overall contribution during the pulse duration from the PM force is considerably stronger than that from the KH force, but their magnitudes differ markedly during the laser pulse. F_{KH} is dominant during both the entrance and exit portions of the laser pulse, whereas F_{PM} peaks at the mid-point of the pulse (t = 0). At the higher frequencies, the peak PM force weakens, and for #3 is overall well below the KH force.

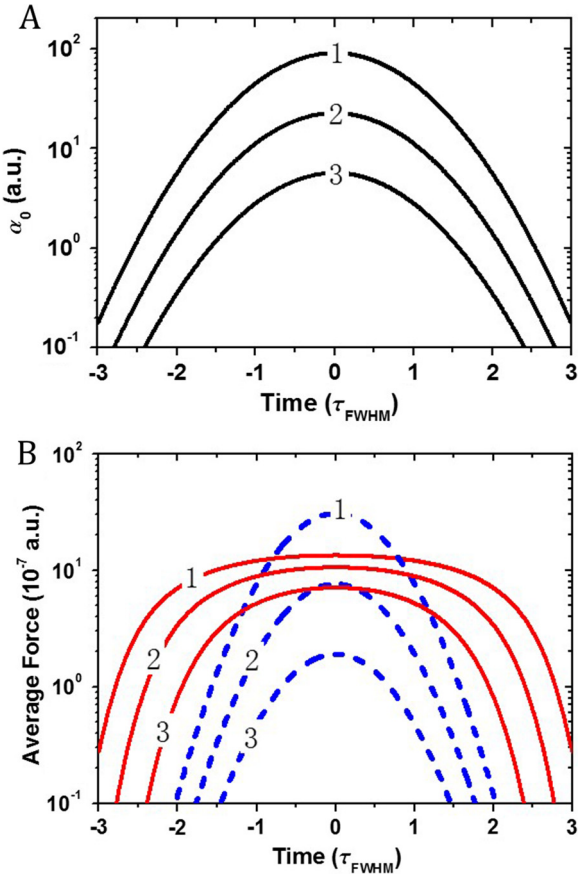

Fig. 3. (A) Dependence on time of the quiver amplitude during the laser pulse envelope (*cf.* below Eq. (6), in units of pulse width, FWHM; reaching maximum at t = 0. Curves labeled 1, 2, 3 pertain to frequencies: ω = 0.056, 0.112, 0.224 a.u., respectively. (B) Maximal radial PM and KH forces, from Eqs. (8) and (12), exerted during the laser pulse on atoms, located at optimal positions within the laser beam (*cf.* Figs 4 and 5). Dashed curves (blue) for PM force, solid (red) for KH force. Laser parameters used are: $I_0 = 2.8 \times 10^{15}$ W cm^{-2}; $w_0 = 17.5$ μm; τ_{FWHM} = 100 fs; wavelengths that correspond to the three frequencies listed in (A) are: $\lambda = 814$ nm (1), 407 nm (2) and 203 nm (3), respectively.

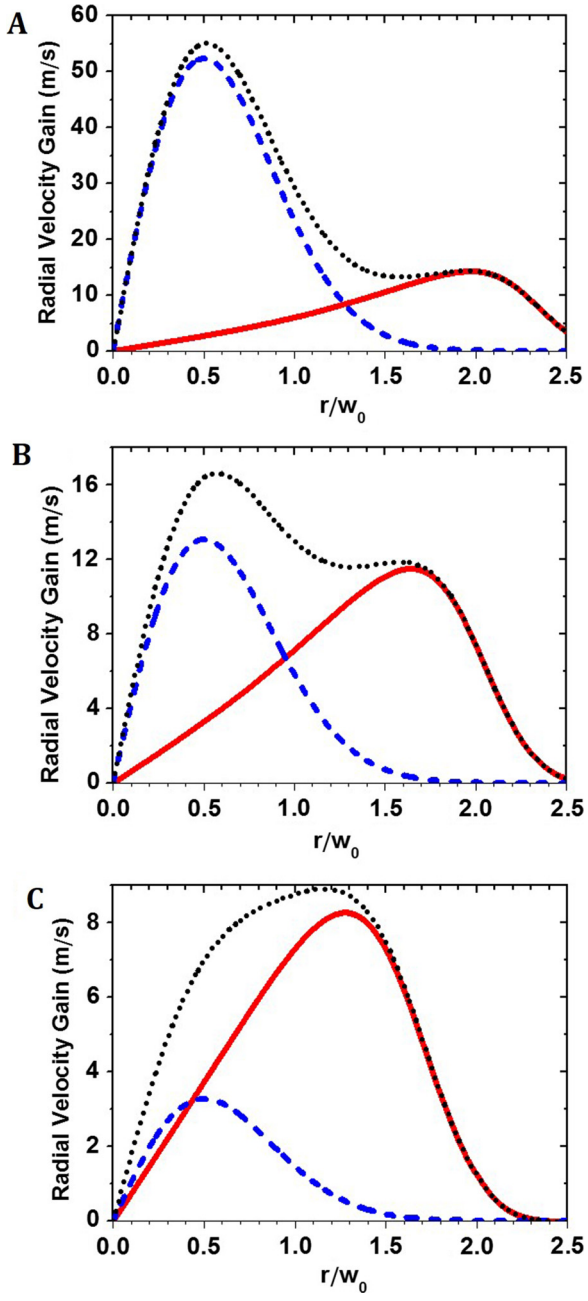

Fig. 4. Velocity gained in the radial direction during the laser pulse to a He atom located at the focal plane (z = 0) as a function of its radial location within the laser beam. Calculated from Eq. (13). Solid curves (red) depict contribution from KH force; dashed (blue) from PM force; dotted (black) total KH + PM. Laser parameters used are: $I_0 = 2.8 \times 10^{15}$ W cm^{-2}; $w_0 = 17.5$ μm; τ_{FWHM} = 120 fs. Panels pertain to laser wavelengths: (A) for $\lambda = 814$ nm; (B) for $\lambda = 407$ nm; (C) for $\lambda = 203$ nm.

4. Velocity gain by atoms

The multichannel position detector (Fig. 1) serves also to determine velocity by time-of-flight [24]. Because momentum is only transferred to the atoms during the laser pulse duration, the initial starting time of the atoms is well defined. The radial deflections of atoms (along the r_D-axis) reaching the detector after each pulse, enable the maximum radial velocity gains to be obtained. Theory gives the radial velocity gain as

$$\Delta V(r,z) = < F_{Tot}(r,z,t) > /M \tag{13}$$

where M is the atom mass, $F_{Tot}(r,z,t)$ the sum of the PM and KH radial forces, from Eqs. (8) and (12), exerted on an atom located at position (r, z) of the intersection of the laser and atom beams. Brackets indicate integration over the pulse envelope duration, giving

$$\Delta V(r,z) = \frac{r}{r_0^2} \cdot \frac{\sqrt{\pi}\tau}{M\omega^2} \left[I(r,z) + 2^{3/2} \sqrt{I(r,z)} \cdot \frac{\partial \epsilon_0}{\partial \alpha_0} \right] \tag{14}$$

where I(r,z) is the spatial portion of Eq. (7). The maximum velocity gain extracted from the experimental data corresponds to the r-location where F_{Tot} is maximal, denoted as $\Delta V_{max}(z)$.

Fig. 4 plots ΔV(r, 0), the radial dependence of the velocity gain at the focal plane, for the PM and KH forces and their sum. Panels A, B, C show results for the three frequencies specified (1, 2, 3) in Fig. 3. In panel A, the maximal Tot force is close to that for the PM force (at r = w_0/2), well removed from that for the KH force (at r ∼ 2 w_0). Increasing the frequency decreases the PM force more rapidly than the KH force, as also evident in Fig. 3B. Also, the peak location and width of the radial dependence of the PM force remain similar, whereas those of the KH force shift markedly. Accordingly, the maximal Tot force weakens and shifts outward, so $\Delta V_{max}(0)$ decreases in magnitude and occurs at wider radial locations (in panel C, at r ∼ 1.2 w_0).

Fig. 5 augments Fig. 4A by showing the distributions of the radial velocity gain ΔV(r, z) transferred to atoms located outside

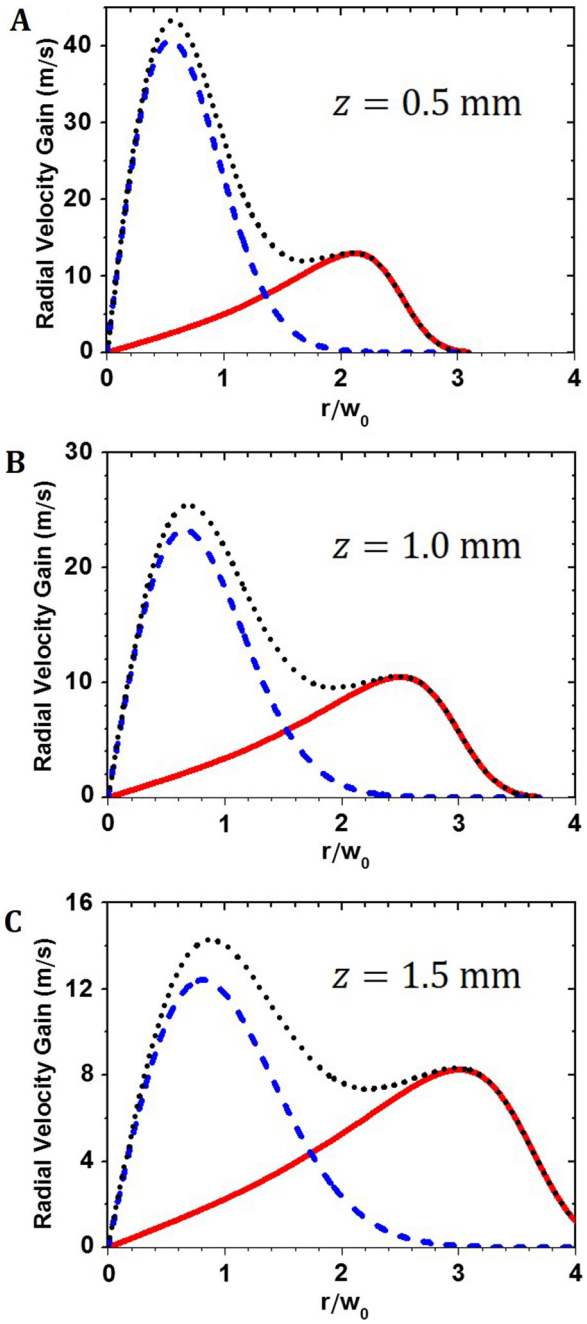

Fig. 5. Companion plot to Fig. 4A, exhibiting velocity in the radial direction transferred to a He atom as a function of its radial location at various positions along the laser beam axis: z = 0.5 mm, 1.0 mm. 1.5 mm.

the focal plane at z = 0.5, 1.0 and 1.5 mm. The further away the atoms are, the more the force distributions shrink in height and broaden in width.

5. Comparison with experiment

The experimental data presented by Eichmann et al. [24] comprises plots of maximum radial velocity gains extracted from observed deflection profiles at the position detector for constant laser peak intensity but with five different pulse durations. These were compared with PM force calculations which used r = w_0/2, the location for maximal force at the focal plane (z = 0).

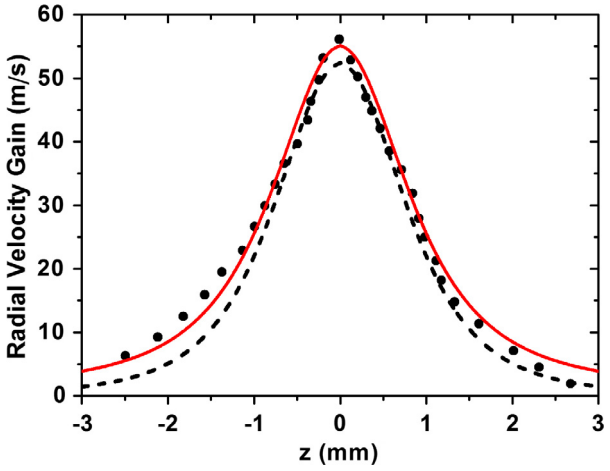

Fig. 6. Experimental data (black points) for maximum velocity in the radial direction gained by He atoms distributed along the laser beam direction (z-axis), compared with model theory results. Dashed curve (black) obtained from [24] for PM force only. Full curve (red) from Eq. (13) for sum of PM and KH forces, from maxima of radial locations from Figs 4 and 5. The experimental data are from Fig. 2, panel e, in [24]. The laser parameters are the same as in our Fig. 4A. As the force along the laser beam direction (z-axis) is negligible, the $\Delta V_{max}(z)$ as imaged at the detector along the z_D-axis arises from the width of the atom beam. That includes spreading due to divergence en route which was accounted for in the data analysis [24].

Fig. 6 shows a sample of their $\Delta V_{max}(z)$ data (black points) for He and the PM calculation (dashed black curve) for z ranging between ±3 mm. We supplied a calculation (solid red curve) using Eq. (14), which includes both PM and KH forces. For both calculations agreement with experiment is satisfactory, so offer no evidence for the KH force.

Fig. 7 plots for He and Ne atoms their $\Delta V_{max}(0)$ data (black dots) pertaining to the focal plane vs. the pulse durations from 40 to 120 fs, again together with a PM calculation (dashed line). The PM predictions lie somewhat below the experimental results. The PM + KH calculations (diamond points and solid red lines) agree well with experiment, but the improvement over PM for He is only modestly outside the uncertainty range and for Ne definitely within it.

Fig. 8 recasts the data and theory of Fig. 7 in a more compact way, by scaling that cancels out the atom mass and pulse duration factors. Panel (A) pertains to the frequency used in the experiment. Agreement is good between He and Ne and between experimental and PM+KH theoretical results; also between different laser pulse durations, although a deviation appears for the 40 fs case. Panel (B) compares theoretical results for the three laser frequencies considered in Figs. 3 and 4, exhibiting that the role of the KH force is markedly enhanced by increasing the frequency.

6. Conclusion

The impetus for this study was our admiration for the work of Eichmann et al. [22–28], both experimental and interpretive, which renewed our interest in the KH atom [1–10]. Indeed, in [24] it is suggested "that a different but equivalent description of our process might be given" in terms of the KH atom, and "our observations of accelerated neutral atoms seem to be a direct confirmation of the existence of this exotic type of stable atom." The acceleration experiment certainly offers another means to pursue the KH atom. However, the ponderomotive force as such is not unique to the KH atom. That led us to work out the force arising from the binding energy of the KH atom.

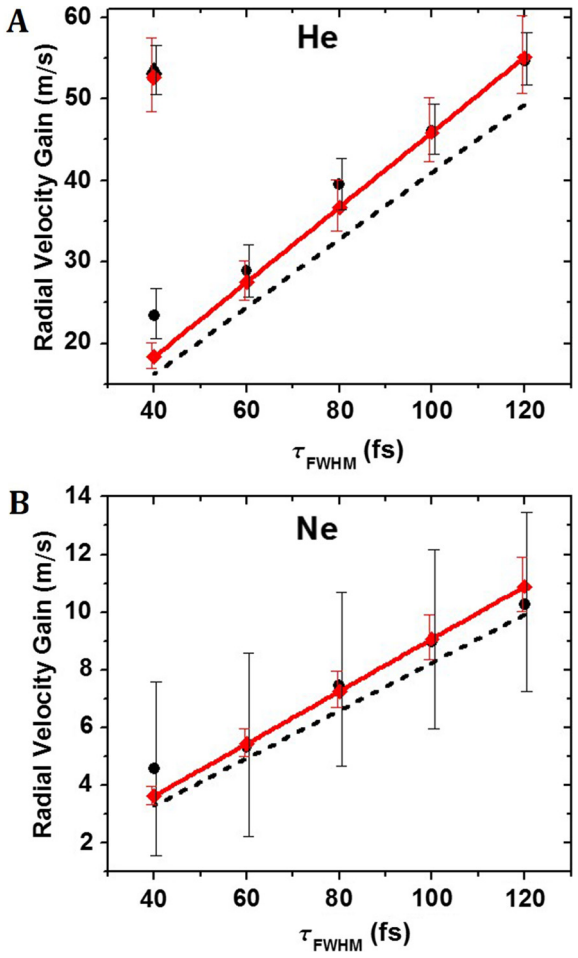

Fig. 7. Maximum radial velocity transferred (A) to He and (B) to Ne atoms located at the focal plane ($z = 0$) as a function of laser pulse duration at constant laser intensity. Circle dots (black) with attached error bars are experimental data from Ref. [24]. Dashed lines (black) show theoretical results given in [24] including only the PM force, and calculated for atoms located at the half-beam site ($r = w_0/2$), which receive the maximum PM force. Diamond points and solid lines (red) are from our theoretical calculations, including both PM + KH force contributions, for atoms at the Tot radial distribution of Fig. 4A (very near $r = w_0/2$). Bars (red) attached to diamond points show range corresponding to the uncertainty of the laser beam waist (bar top $w_0 = 16$ μm, bottom 19 μm). Laser parameters are same as in Fig. 4A except for variation of the pulse durations. *Note*: in upper left corner of (A) the triangle (black) shows experimental datum for $I_0 = 8.3 \times 10^{15}$ W cm^{-2} and $\tau_{FWHM} = 40$ fs, obtained from Fig. 2f of Ref. [24]; diamond (red) is our corresponding theoretical result.

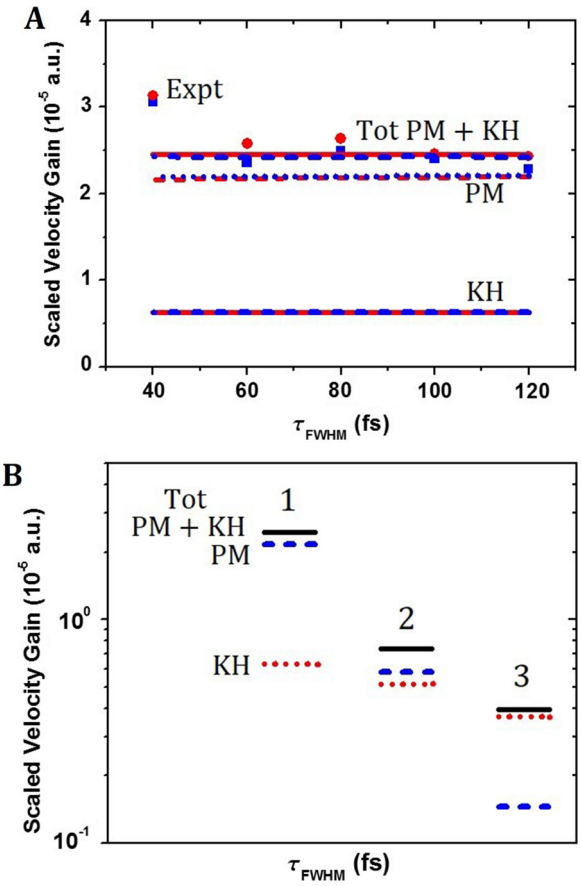

Fig. 8. Radial velocity gain, $M\Delta V/\tau$, scaled by mass of atoms and laser duration. (A) Scaled results obtained from Fig. 7, with laser parameters used in the experiment. For Total PM + KH: *Experimental* results shown with circle dots (red) for He; squares (blue) for Ne; *Theoretical* results shown with solid line (red) for He; dashed line (blue) for Ne. Separate PM and KH contributions shown by dashed lines (red) for He, by dotted line (blue) for Ne. (B) Predicted results for the three laser frequencies considered in Figs. 3 and 4, here labeled 1, 2, 3. Their ratios are 1, 2, 4.

For the experimental parameters used in [24], the KH force is outweighed by the PM force. At present, adding the KH term only gave teasing evidence for the KH atom. A much more incisive test of the KH force can be had by increasing the laser frequency. As seen in Fig. 8B, column 2, doubling the frequency predicts the KH and PM forces would contribute about equally to the velocity gain; in column 3, doubling again and KH would much outweigh the PM force.

Our application of the KH frame to the acceleration of laser-dressed atoms provides a simple illustration of its prospective utility. Current lasers [32,33] offer suitable parameters that will enable a variety of kindred acceleration experiments capable of obtaining firm evidence for the KH atom. A reviewer praised our paper as a "most useful introduction" to the KH atom, but expressed concern that it is "likely necessary to quantize the radiation field" to obtain a more rigorous treatment. That concern was allayed long ago [2,34]. Super-intense lasers deliver immense numbers of photons, thereby making the quantized field equivalent to the familiar classical or semiclassical theory. In a broader context, by producing forces that drastically alter electronic structure, super-intense lasers can much enhance the scope of chemical dynamics.

Acknowledgements

We are grateful for support from Shanghai National Science Foundation (Grant 15ZR1411300) and from National Natural Science Foundation of China (Grant 11674098). Q.W. thanks Wenxue Li for enlightening discussion of lasers. D.H. appreciates the opportunity to discuss the KH atom with Ulli Eichmann and Felipe Morales of the Max Born Institute, Berlin, and members of the Institute for Quantum Science and Engineering, Texas A&M University.

Appendix

To facilitate evaluating the KH force from Eq. (12), we provide a formula for $d\epsilon_0/d\alpha_0$, fitted to the numerical results shown in Fig. 2, for He and Ne atoms:

$$ln(d\epsilon_0/d\alpha_0) = A_0 + A_1 \exp(-\alpha_0/b_1) + A_2 \exp(-\alpha_0/b_2). \quad (15)$$

To obtain the explicit r-dependence of the factor $d\epsilon_0/d\alpha_0$ in Eq. (12) requires inverting Eq. (7), which gives

$$r = r_0\{ln[(I_0^{1/2}/w^2)(r_0/w_0)] - ln\alpha_0\}^{1/2} \quad (16)$$

Parameters	Values: He	Ne
A_0	−8.8838	8.8666
A_1	3.04904	2.9971
b_1	3.01346	2.8682
A_2	5.37583	5.3981
b_2	36.9075	36.3812

R^2 = 0.9994 for fittings of both He and Ne.

References

[1] M. Gavrila, Atoms in Intense Laser Fields, Academic Press, New York, 1992.
[2] J.H. Eberly, K.C. Kulander, Atomic stabilization by super-intense lasers, Science 262 (1993) 1229.
[3] M. Gavrila, Topical Review: Atomic stabilization in superintense laser fields, J. Phys. B: At Mol. Opt. Phys. 35 (2002) R147.
[4] E. van Duijn, M. Gavrila, H.G. Muller, Multiply charged negative ions of hydrogen induced by superintense laser fields, Phys. Rev. Lett. 77 (1996) 3759.
[5] Q. Wei, S. Kais, N. Moiseyev, New stable multiply charged negative atomic ions in linearly polarized superintense laser fields, J. Chem. Phys. 124 (2006) 201108.
[6] Q. Wei, S. Kais, N. Moiseyev, Frequency-dependent stabilization of He− by a superintense laser field, Phys. Rev. A 76 (2007) 013407.
[7] Q. Wei, S. Kais, D. Herschbach, Dimensional scaling treatment of stability of atomic anions induced by superintense high-frequency laser fields, J. Chem. Phys. 129 (2007) 214110.
[8] Q. Wei, D. Herschbach, Positronium in superintense high-frequency laser fields, Mol. Phys. 111 (2013) 1835.
[9] T. Yasuike, K. Someda, He–He chemical bonding in high-frequency intense laser fields, J. Phys. B: At Mol. Opt. Phys. 37 (2004) 3149.
[10] Q. Wei, S. Kais, D. Herschbach, Dimensional scaling treatment of stability of simple diatomic molecules induced by super- intense, high-frequency laser fields, J. Chem. Phys. 129 (2008) 214110.
[11] O. Smirnova, M. Spanner, M. Ivanov, Molecules without Electrons: binding bare nuclei with strong laser fields, Phys. Rev. Lett. 90 (2003) 243001.
[12] P.L. Kapitza, Collected Papers, in: D. Ter Haar (Ed.), Vol. 2, Pergamon, Oxford, 1965.
[13] W. Paul, Electromagnetic traps for charged and neutral particles, Rev. Mod. Phys. 62 (1990) 531.
[14] L.V. Hau, M.M. Burns, J.A. Golovchenko, Bound states of guided matter waves: an Atom and a charged wire, Phys. Rev. A 45 (1992) 6468.
[15] H.A. Kramers, Collected Scientific Papers, North-Holland, Amsterdam, 1956, p. 866.
[16] W.C. Henneberger, Perturbation method for atoms in intense light beams, Phys. Rev. Lett. 21 (1968) 838.
[17] M. Richter, Imaging and Controlling Electronic and Nuclear Dynamics in Strong Laser Fields, Ph.D. Thesis, Tecnischen Universitat Berlin, 2016.
[18] A.M. Popov, M.A. Tikhonov, O.V. Tikhonov, E.A. Volkova, Comparative analysis of the strong-field ionization of a quantum system with the Coulomb and short-range potentials, Laser Phys. 19 (2009) 191.
[19] M. Stroe, I. Simbotin, M. Gavrila, Low-frequency atomic stabilization and dichotomy in superintense laser fields: full Floquet results, Phys. Rev. A 78 (2008) 033405.
[20] F. Morales, M. Richter, S. Patchkovskii, O. Smirnova, Imaging the Kramers-Henneberger atom, Proc. Natl. Acad. (USA) 108, 16906 (2011).
[21] M. Richter, S. Patchkovskii, F. Morales, O. Smirnova, M. Ivanov, The role of the Kramers-Henneberger atom in the higher-order Kerr effect, New J. Phys. 15 (2013) 083012.
[22] N.J. van Druten, R.C. Constantinescu, J.M. Schins, H. Nieuwenhuize, H.G. Muller, Adiabatic stabilization: observation of the surviving population, Phys. Rev. A 55 (1997) 622.
[23] T. Nubbemeyer, K. Gorling, A. Saenaz, U. Eichmann, W. Sandner, Strong-field tunneling without ionization, Phys. Rev. Lett. 101 (2008) 233001.
[24] U. Eichmann, T. Nubbemeyer, H. Rottke, W. Sandner, Acceleration of neutral atoms in strong short-pulse laser pulse fields, Nature 461 (2009) 1261.
[25] U. Eichmann, A. Saenz, S. Eilzer, T. Nubbemeyer, W. Sandner, Observing rydberg atoms to survive intense laser fields, Phys. Rev. Lett. 110 (2013) 203002.
[26] S. Eilzer, H. Zimmermann, U. Eichmann, Strong-field Kapitza-Dirac scattering of neutral atoms, Phys. Rev. Lett. 112 (2014) 113001.
[27] S. Eilzer, U. Eichmann, Steering neutral atoms in strong laser fields, J. Phys. B: At. Mol. Opt. Phys. 47 (2014) 204014.
[28] H. Zimmermann, J. Buller, S. Eilzer, U. Eichmann, Strong field excitation of he: bound state distribution and spin effects, Phys. Rev. Lett. 114 (2015) 123003.
[29] M. Førre, S. Selstø, J.P. Hansen JP, L.P. Madsen, Exact nondipole Kramers-Henneberger form of the light-atom Hamiltonian: an application to atomic stabilization and photoelectron energy spectra, Phys. Rev. Lett. 95 (2005) 043601.
[30] A.V. Sergeev, S. Kais, Critical nuclear charges for N-electron atoms., Int'l. J. Quantum Chem. 75, 533 (1999).
[31] P.X. Wang, Q. Wei, P. Cai, J.X. Wang, Y.K. Ho, Neutral particles pushed or pulled by laser pulses, Opt. Lett. 41 (2016) 230.
[32] P. Gibbon, Short Pulse Interactions with Matter: An Introduction, World Scientific Publishing Co., Singapore, 2005.
[33] J.C. Deils, W. Rudoph, Ultrashort Laser Pulse Phenomea, Academic Press, New York, 2006.
[34] H.R. Reiss, Foundations of Strong-Field Physics, in Lectures of Ultrafast Intense Laser Science, in: K. Yamanouchi (Ed.), Springer Series in Chemical Physics, 2010, p. 79.